Frequency Support from PMSG-Based Wind Turbines with Reduced DC-Link Voltage Fluctuations

Jiafa He, Linbin Huang, Di Wu, Chengzhi Zhu, and Huanhai Xin
(Invited)

***Abstract*—Frequency droop control is widely used in permanent magnet synchronous generators (PMSGs) based wind turbines (WTs) for grid frequency support. However, under frequency deviations, significant DC-link voltage fluctuations may occur during the transient process due to sudden changes in real power of such WTs. To address this issue, a current feedforward control strategy is proposed for PMSG-based WTs to reduce DC-link voltage fluctuations when the WTs are providing frequency support under grid frequency deviations. Meanwhile, the desired frequency support capability of the PMSG-based WTs can be ensured. Simulation results verify the rationality of the analysis and the effectiveness of the proposed control method.**

***Index Terms*—Current feed forward control, DC-link voltage, frequency droop control, frequency support, PMSG-based WTs.**

I. INTRODUCTION

THE increasing penetration of wind power in modern power grids can lead to the reduced inertia of power systems, which has drawn considerable attentions from system operators [1]. As a result, wind turbines (WTs) are gradually required to participate in the grid frequency regulation and provide active power support under frequency disturbances [2].

Conventional control strategies of the WTs aim to extract the maximum active power from the grid using maximum power point tracking (MPPT) algorithms [3]. In this manner, the WT cannot provide additional active power support when the grid frequency fluctuates, which will result in the decrease of the power system inertia and weaken the frequency regulation capability [4]. Therefore, frequency regulation strategies, such as inertial emulation and primary frequency control, are widely adopted for the WTs.

These strategies commonly introduce the grid frequency differential signal (i.e., *df/dt*) and the frequency deviation signal (i.e., Δf) into the WT's power control or torque control [5]-[6]. Based on these strategies, the WT's active power output can respond to the grid frequency disturbances, which will release the stored kinetic energy of the rotating mass to support the power grid [7]. Ref.[8] further utilized the *df/dt* term to design a novel control structure, in which the WT can provide frequency support and positive damping during frequency and oscillation events. In [9], effects of a droop control strategy, using the Δf term to realize the frequency support for the WT, is investigated, and the influence of control parameters on the frequency support capability is particularly discussed.

When these frequency regulation strategies are applied in permanent magnet synchronous generator (PMSG) based WTs, which are connected to the grid via a back-to-back structure with a DC-link capacitor [10], one major concern is that these strategies can cause fluctuations of the DC-link voltage under frequency disturbances. This voltage fluctuation results from the power imbalance of the DC-link capacitor, which will be particularly analyzed in this paper. Note that this DC-link voltage fluctuation should be prevented as it can lead to the damage of the DC-link capacitor and the failure of the power transmission. However, to our best knowledge, most existing literatures focus on the control design for PMSG-based WTs to improve the frequency support capability [11], and how to reduce the DC-link voltage fluctuations resulting from these frequency regulation strategies has not been well discussed and designed.

To deal with this problem, a current feedforward control (GCFC) scheme is proposed for PMSG-based WTs in this paper, in which the current signal of the generator-side converter is introduced to modify the current reference signal of the grid-side converter. The proposed GCFC can suppress the DC-link voltage fluctuation effectively for PMSG-based WTs under grid frequency disturbances. The control design and implementation of the GCFC are presented in detail in this paper, and the mechanism of suppressing the DC-link voltage fluctuation is analyzed in particular. With the GCFC, the DC-link voltage fluctuation can be kept within its admissible range; meanwhile, the desired frequency support capability of

Manuscript was submitted for review on 03, September, 2018.

This work is jointly supported by the National Key R&D Programme of China (No. 2017YFB0902000), the National Natural Science Foundation of China(No.U1766206) and the Science and Technology Programme of the State Grid Corporation (No.52110418000P).

Jiafa He, Linbin Huang and Huanhai Xin are with the College of Electrical Engineering, Zhejiang University, Hangzhou 310027, China (emails: xinhh@zju.edu.cn, jiafa_he@zju.edu.cn).

Chengzhi Zhu is with the State Grid Zhejiang Electric Power, Co., LTD, Hangzhou 310014, China.

Di Wu is with the D. Wu is with the Department of Electrical and Computer Engineering, North Dakota State University, Fargo 58102, USA. (email: di.wu.3@ndsu.edu).

Digital Object Identifier 10.30941/CESTEMS.2018.00037

the PMSG-based WT can be ensured.

II. Control of PMSG-Based WTs

In this section, the basic control structure of PMSG-based WTs is firstly introduced, with the frequency droop control applied for grid frequency support. Then, the implementation of the GCFC is presented.

Fig.1 shows an one-line diagram of a PMSG-based WT system connected to a three-phase ac grid, where P_{wind} is the captured wind power, P_{WT} is the generator's power output, P_g is the grid-side converter's active power transmitted to the grid, V_s and I_s are magnitudes of the stator's voltage and current output, respectively. V_g and I_g are magnitudes of the grid-side converter's voltage and current output, respectively, V_{DC} is the DC-link voltage, ω_r is the rotor speed and f_{PLL} is the PLL frequency output. Note that the active power output of the WT can be controlled via either the generator-side converter or the grid-side converter [12], and it's chosen to be controlled by the generator-side converter in this paper.

In this way, the MPPT algorithm and the frequency droop control are implemented in the generator-side controller [12], and the grid-side controller performs DC-link voltage control. The detailed dynamic model of the WT system and the associated converters can be found in [13].

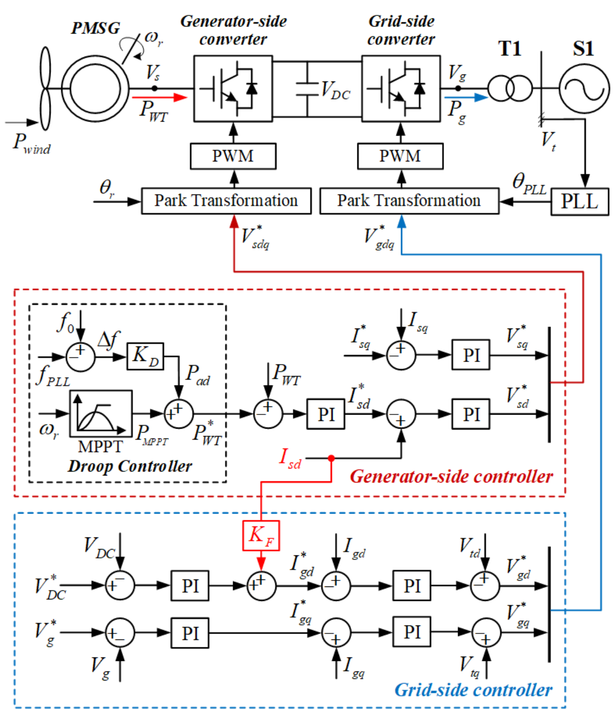

Fig. 1. One-line diagram of a grid-connected PMSG-based WT.

A. Generator-Side Converter Control

In the control of the generator-side converter, the frequency droop controller introduces the frequency deviation signal (Δf) into the active power reference to build a relationship between the generator's power output and the grid frequency, as depicted in Fig.1. The basic control strategy is

$$\begin{aligned} P_{WT}^{*} &= P_{MPPT} + P_{ad} = P_{MPPT} + K_D \Delta f \\ &= P_{MPPT} + K_D \left(f_0 - f_{PLL} \right) \end{aligned} \tag{1}$$

where P_{WT}^{*} is the new reference of the generator's power output, P_{MPPT} is the active power reference calculated by the MPPT algorithm according to the rotor speed ω_r, P_{ad} is the additional power deviation, K_D is the droop coefficient, f_0 is the frequency reference. Note that the additional power deviation P_{ad} can be obtained by two main controllers. One is the proportional (P) controller, and the other one is the derivative (D) controller. Since the D controller may cause the instability due to the noises in the frequency measurement [8], this paper only utilizes the P controller as a frequency regulation strategy for the WT.

Eqn.(1) shows that the value of P_{WT}^{*} is coupled with the grid frequency deviation ($\Delta f = f_0 - f_{PLL}$). That is, under the grid frequency dips, P_{WT}^{*} will deviate from P_{MPPT} in order to release the kinetic energy stored in rotating masses to support the grid frequency. And under frequency rise, the WT will absorb active power to provide frequency support for power grid. Moreover, the droop coefficient K_D can influence the rate of change of active power output under grid frequency deviations, which will be further studied in Section IV-B.

Since the design of the inner current control loop has been involved in many literatures [10], it is not discussed here due to the limited space.

B. Grid-Side Converter Control

The grid-side converter controls the DC-link voltage within the admissible range in order that the two converters can operate pulse-width modulation (PWM). In this paper, two cascaded control loops are used in the grid-side converter. And this cascade control structure has been studied in many literatures such as [14] and [15], which is widely adopted for voltage source converters (VSCs) [16]. To be specific, the outer voltage loop controls the DC-link voltage V_{DC} and the converter voltage magnitude V_g and the inner current loop regulates the *d-axis* current I_{gd} and the *q-axis* current I_{gq} to their references, which can be expressed as:

$$\begin{cases} V_{gd}^{*} = V_{td} - H_I(s) \times \left(I_{gd} - I_{gd}^{*} \right) \\ V_{gq}^{*} = V_{tq} - H_I(s) \times \left(I_{gq} - I_{gq}^{*} \right) \end{cases} \tag{2}$$

Where I_{gd}, I_{gq} are the *dq*-axis current of the grid-side converter, I_{gd}^{*}, I_{gq}^{*} are the *dq*-axis current reference of the grid-side converter. $H_I(s) = K_{IP} + K_{II}/s$ is the transfer function of the PI controller for the inner current loop.

C. GCFC Scheme

The GCFC scheme is applied in the grid-side controller, as shown in Fig.1. The basic control strategy is

$$I_{gd}^{*} = H_{DC}(s) \times \left(V_{DC}^{*} - V_{DC} \right) + K_F I_{sd} \tag{3}$$

where $H_{DC}(s)=K_{DCP}+K_{DCI}/s$ is the transfer function of the PI controller for the DC-link voltage controller, I_{sd} is the *d-axis* current of the generator-side converter associated with the generator's power output, and K_F is the feedforward coefficient.

The GCFC scheme introduces the *d-axis* current I_{sd} of the generator-side converter to modify the *d-axis* current reference I_{gd}^* of the grid-side converter. The effects of the GCFC scheme on the DC-link voltage fluctuations will be analyzed in the next section.

III. Dynamic Behaviors of PMSG-Based WTs Under Frequency Disturbances

A. Frequency Support From PMSG-Based WTs

In the electromechanical timescale, the generator's power output can be approximated by its reference value P_{WT}^*, which is determined by the MPPT algorithm and the frequency droop control. That is, $P_{WT}\approx P_{WT}^*$. Subsequently, the generator rotor's dynamic function can be expressed as

$$2H_s\omega_r\frac{d\omega_r}{dt}=P_{wind}-P_{WT}^* \tag{4}$$

where H_s is the mechanical inertia constant of the generator.

Substituting (1) into (4) yields

$$2H_s\omega_r\frac{d\omega_r}{dt}=P_{wind}-\left(P_{MPPT}+K_D\Delta f\right) \tag{5}$$

Based on Eqn.(5), the WT's operating characteristics under grid frequency deviations can be obtained, as shown in Fig.2. The detail mathematical expression of P_{wind} can be found in [8].

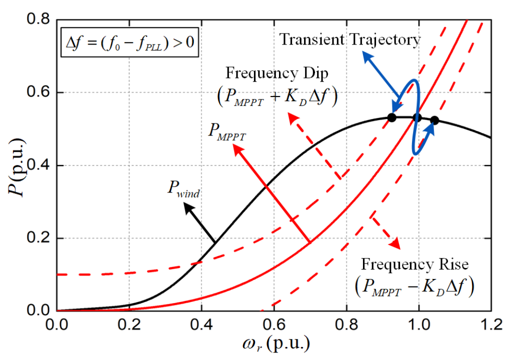

Fig. 2. Transient responses of the WT under grid frequency deviations.

It can be seen from Fig.2 that under the grid frequency dip, the red solid line, which represents power reference outputted from the MPPT algorithm, will change to the red dash line due to the frequency droop control and the rotor speed ω_r will decrease to a new equilibrium, and during the transient process, the PMSG-based WT will release the kinetic energy stored in the rotating mass to provide frequency support to the grid. After the transient process, the WT's active power output in the new equilibrium is less than the original point due to the deviation of P_{WT} from the MPPT curve under the grid frequency dip. On the other hand, under frequency rise, it can be seen from Fig.2 that the WT will experience an acceleration process and absorb active power to provide frequency support for power grid. The rotor speed of the new equilibrium may exceed the admissible range under severe frequency rise, but the pitch angle controller will work to lower the rotor speed in this scenario and prevent from overspeed. The transient responses of the PMSG-based WTG with frequency droop control under frequency deviations will be further verified by simulation results in Section V.

B. DC-Link Voltage Fluctuations of PMSG-Based WTs

The frequency droop control in (1) sets a relationship between the generator's power output reference P_{WT}^* and the grid frequency deviation Δf, which can utilize the kinetic energy stored in the WT's rotating masses for frequency support. In this way, the generator's active power output P_{WT} will change accordingly under grid frequency deviations. However, the change of P_{WT} will cause the power imbalance of the DC-link capacitor and result in the DC-link voltage fluctuation, since the dynamic equation of the DC-link capacitor in (6) shows that the change of P_{WT} will lead to the change of dV_{DC}/dt. Note that in Eqn.(6), C_{DC} is the DC-link capacitor.

$$C_{DC}\frac{dV_{DC}}{dt}=\frac{P_{WT}}{V_{DC}}-\frac{P_g}{V_{DC}} \tag{6}$$

Eqn. (6) can be further written as

$$\frac{C_{DC}}{2}\frac{d\left(V_{DC}\right)^2}{dt}=\frac{C_{DC}}{2}s\left(V_{DC}\right)^2=P_{WT}-P_g \tag{7}$$

The DC-link voltage fluctuation will change the PI's output of the DC-link voltage controller i.e., I_{gd}^*, as illustrated in Fig.3 (a). Then, the grid-side converter's power output P_g will be changed accordingly (since $P_g\propto I_{gd}^*$ holds in steady state, similar to [17]) to regulate the DC-link voltage as a negative feedback, depicted in Fig.3 (b). It can be deduced from Fig.3 (a) that the DC-link capacitor act as a buffer to transmit the active power from the generator to the grid, which can cause the DC-link voltage fluctuation in the case of power imbalance.

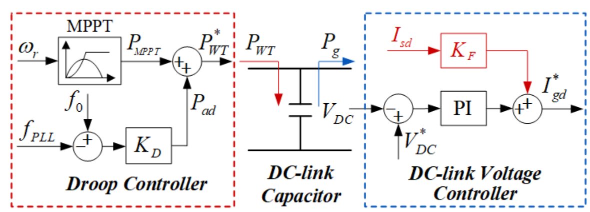

(a)

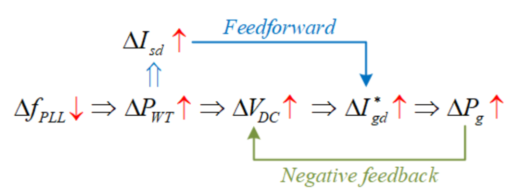

(b)

Fig. 3. Dynamics of the DC-link capacitor.

C. Suppressing DC-link Voltage Fluctuations by GCFC

The voltage vector of the grid-side converter is oriented at the controller *d-axis* by applying a conventional PLL [17], as shown in Fig.1. Therefore, the steady state values of P_{WT} and P_g can be calculated by

$$P_{WT}=V_sI_{sd}\quad and\quad P_g=V_gI_{gd} \tag{8}$$

To simplify the analysis of the GCFC's effect, we ignore the dynamics of the inner current control loop in the grid-side converter, so there is $I_{gd}^* = I_{gd}$, similar to [17].

Then, substituting (3), (8) and $I_{gd}^* = I_{gd}$ into (6) yields

$$\begin{aligned} C_{DC}V_{DC}\frac{dV_{DC}}{dt} &= V_s I_{sd} - V_g\left[H_{DC}(s)(V_{DC}^* - V_{DC}) + K_F I_{sd}\right] \\ &= -V_g H_{DC}(s)(V_{DC}^* - V_{DC}) + (V_s - V_g K_F) I_{sd} \end{aligned} \tag{9}$$

It can be seen from Eqn.(9) that the GCFC can compensate the disturbance of I_{sd} ($I_{sd} \propto P_{WT}$) by choosing a proper value of K_F, which will reduce the DC-link voltage fluctuation. This mechanism is also shown in Fig.3 (b) that the GCFC introduces a feedforward channel in order that the change of P_{WT} will directly cause variations of I_{gd}^*, and thus its impact on the DC-link voltage V_{DC} can be compensated.

IV. Small Signal Analysis

In this section, the closed-loop transfer function of the PMSG-based WT system is firstly given. Then, the influences of the feedforward coefficient and the droop coefficient on the system's dynamic performance are further studied.

A. Closed-loop Transfer Function of PMSG-based WTs

The small signal model of the PMSG-based WT has been well-established in many literatures such as [18] and [19]. Thus, it is omitted here due to the limited space. The dynamics of the WT system in Fig.1 can be represented by the state space equation in (10)

$$\begin{cases} \dot{X} = \boldsymbol{A}X + \boldsymbol{B}u \\ y = \boldsymbol{C}X + \boldsymbol{D}u \end{cases} \tag{10}$$

where X is the state variable vector of the WT system, u is the input signal vector, y is the output signal vector, $\boldsymbol{A}$ is the state matrix, $\boldsymbol{B}$ is the input matrix, $\boldsymbol{C}$ is the output matrix, $\boldsymbol{D}$ is the feedforward matrix. In this paper, the grid frequency deviation Δf is chosen as the input (i.e., $u = \Delta f$) and the DC-link voltage deviation ΔV_{DC} is chosen as the system's output (i.e., $y = \Delta V_{DC}$).

Then, the closed-loop transfer function of the DC-link voltage deviation can be derived, which is

$$\frac{\Delta V_{DC}}{\Delta f} = \boldsymbol{C}(s\boldsymbol{I} - \boldsymbol{A})^{-1}\boldsymbol{B} + \boldsymbol{D} \tag{11}$$

The dynamics of the DC-link voltage under grid frequency deviations is dominated by the transfer function given in (11). Therefore, the closed-loop transfer function can be used to analyze the influences of control parameters on the DC-link voltage's dynamic performance, which is particularly studied in the following.

B. Influences of Control Parameters

Fig.4 shows the closed-loop bode diagram with different values of K_F, where $K_D = 50$. It can be seen from Fig.4 that the infinite norm $H\infty$ decreases from 34.12dB ($K_F = 0$) to 17.24dB ($K_F = 1$) with the increase of K_F, which means the disturbance attenuation capability is improved by increasing K_F [20]. That is, the feedforward coefficient K_F has great influences on the DC-link voltage's dynamic performance and increasing K_F can suppress the DC-link voltage fluctuation.

According to Fig.4, it can be seen that with the feedforward coefficient K_F increase, the infinite norm $H\infty$ decreases. In order to give a perceptual intuition of the relationship between the feedforward coefficient K_F and the infinite norm $H\infty$, the fitting curve is depicted as showed in Fig.5.

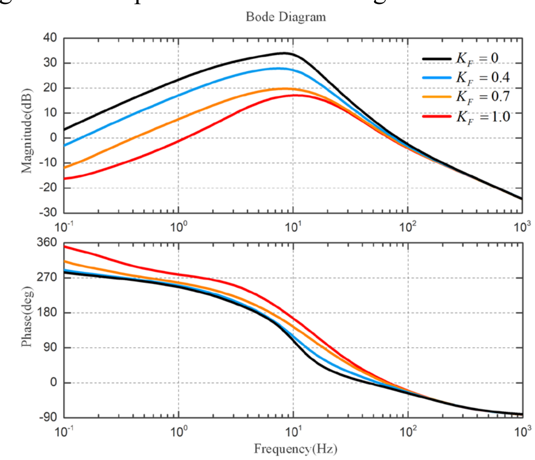

Fig. 4. Closed-loop bode diagram with different values of K_F

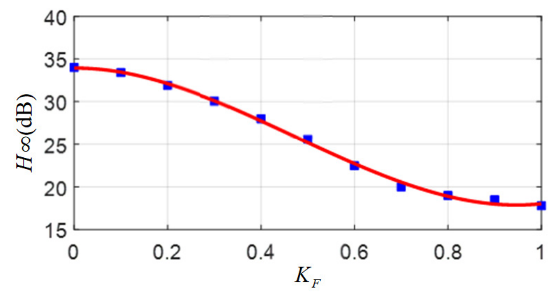

Fig. 5. Fitting curve of the relationship between $H\infty$ and K_F

Fig.6 shows the closed-loop bode diagram with different values of K_D, where $K_F = 0$. It can be seen that with the decrease of K_D, the infinite norm $H\infty$ changes from 38.10dB ($K_D = 80$) to 26.05dB ($K_D = 20$). That is, decreasing the droop coefficient K_D can reduce the DC-link voltage fluctuation. However, with the decrease of K_D, the frequency support capability of the WT is also reduced, which is not desired in practice. Also, the fitting curve is showed in Fig.7.

According to Fig.4 and Fig.6, it can be seen that both K_F and K_D have great influences on the DC-link voltage's dynamic performance. In order to analyze the coordinated impacts of K_F and K_D, we give the infinite norm $H\infty$ as a function of K_F and K_D in Fig.8. It can be seen that $H\infty$ increases with the decrease of K_D, and $H\infty$ decreases with the increase of K_F.

In practice, the value of K_D should be tuned according to the desired frequency support capability of the WT, and a larger value improves the frequency support capability, which can lead to great DC-link voltage fluctuations if $K_F = 0$ (i.e., the GCFC is not applied), as deduced from Fig.8. This problem can be dealt with by applying the GCFC and increasing K_F, since the increase of K_F plays a positive role in reducing DC-link voltage fluctuations as shown in Fig.8. In other words, the GCFC provides an additional degree of freedom to improve the dynamics of the DC-link voltage without reducing the frequency support capability of the WT.

Based on the small signal model of the PMSG-based WT established in Section IV-A, the active power close-loop transfer function can be derived by utilizing the state space (10), which is similar to the deducing process of the DC-link voltage deviation close-loop transfer function (11). The input of active power loop transfer function is P_{WT} and the output is P_g. Therefore, the closed-loop bode diagram can be depicted as showed in Fig. 9. It can be seen from Fig. 9 that a big resonance peak appears on the amplitude-frequency curve when $K_F = 0$ and the peak drops with the increase of K_F. That is, the current feedforward coefficient K_F has great influence on the dynamic performance of the active power. This dynamic performance can affect the deviation between P_{WT} and P_g during the transient process, which can further change the value of dV_{DC}/dt and influence the DC-link voltage's dynamic performance, as described in (6). Therefore, increasing K_F can improve the active power's dynamic performance and then reduce the DC-link voltage fluctuation.

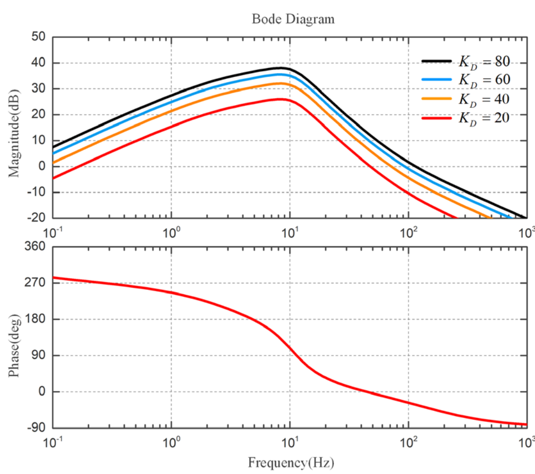

Fig. 6. Closed-loop bode diagram with different values of K_D

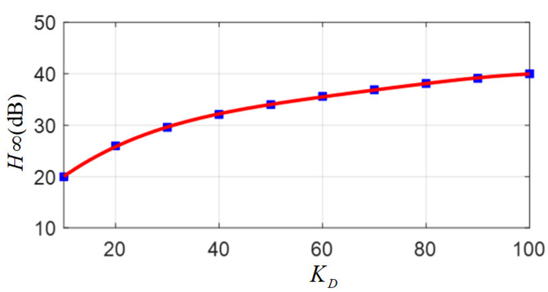

Fig. 7. Fitting curve of the relationship between $H\infty$ and K_D

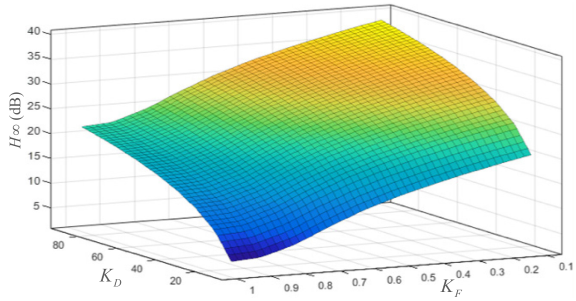

Fig. 8. Infinite norm $H\infty$ with different values of K_F and K_D

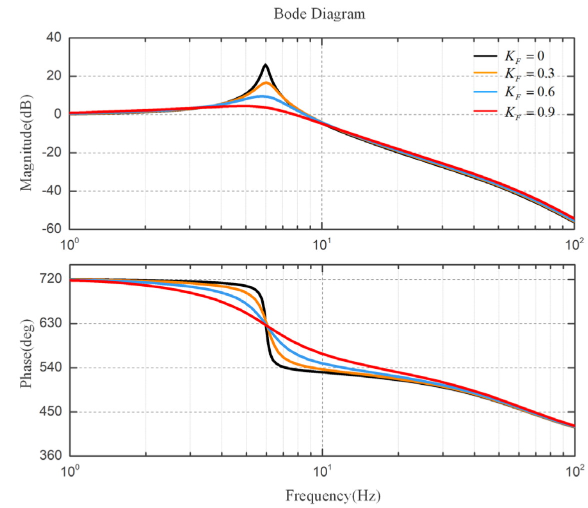

Fig. 9. Active power closed-loop bode diagram with different values of K_F

V. Simulation Validation

To further verify the validity of the aforementioned analysis and the effectiveness of the proposed GCFC, simulations based on MATLAB/Simulink are carried out on the PMSG-based WT system in Fig.1. The ac grid in Fig.1 is simulated by a three-phase voltage source with fixed amplitude and frequency. The main parameters are set as follows: the rated voltage $V_{nom} = 690\text{V}$, the rated power $P_{nom} = 1.5\text{MW}$, the rated frequency $f_{nom} = 50\text{Hz}$, the *dq-axis* inductances of the PMSG-based WT $L_d = L_q = 1.387\text{p.u.}$, the DC-link capacitor $C_{DC} = 0.12\text{p.u.}$, the inertia constant $T_a = 10.459s$, the number of pole pairs $P = 48$.

Assuming that the grid frequency drops at t=1s, which is realized by programing the grid frequency to step from 50Hz to 49.8Hz, the time-domain responses of the PMSG-based WT with different values of K_D are given in Fig.10. Under the frequency dip, the power output P_g increases rapidly for frequency support. With the increase of K_D, the power output increases to provide more additional power to the grid, but the DC-link voltage fluctuation is also increased, as shown in Fig.10, which is consistent with the analysis in Section IV-B.

To further investigate the influence of the GCFC on suppressing the DC-link voltage fluctuation, the PMSG-based WT's responses with different values of K_F under the frequency dip are given in Fig.11. With the increase of K_F from 0 to 1, the DC-link voltage fluctuation is reduced greatly and the power output remains the same, which means that the proposed GCFC can effectively suppress the DC-link voltage fluctuation and simultaneously, ensure the desired frequency support capability of the PMSG-based WT.

On the other hand, in order to investigate the frequency support capability of the PMSG-based WT under grid frequency rise, we assume that the grid frequency raises at t=1s, which is realized by programming the grid frequency to step from 50Hz to 50.2Hz, the time-domain responses of the

PMSG-based WT with different values of K_D are given in Fig.12. Under the frequency rise, the power output P_g decreases rapidly and the WT experiences an acceleration process and absorb active power to provide frequency support for power grid. With the increase of K_D, the power output decreases to absorb more power from the grid, but the DC-link voltage fluctuation is increased.

Under the same disturbance of grid frequency, the responses of the PMSG-based WT with different values of K_D are shown in Fig.13. With the increase of K_D from 0 to 1.0, the power output P_g decreases to the same degree. Meanwhile, the fluctuation of DC-link voltage is significant decreased under grid frequency rise with the proposed current feedforward control, which is consistent with the analysis in Section IV-B. Therefore, the responses in Fig.13 verify the effective suppression for the DC-link voltage fluctuation under both grid frequency dip and rise.

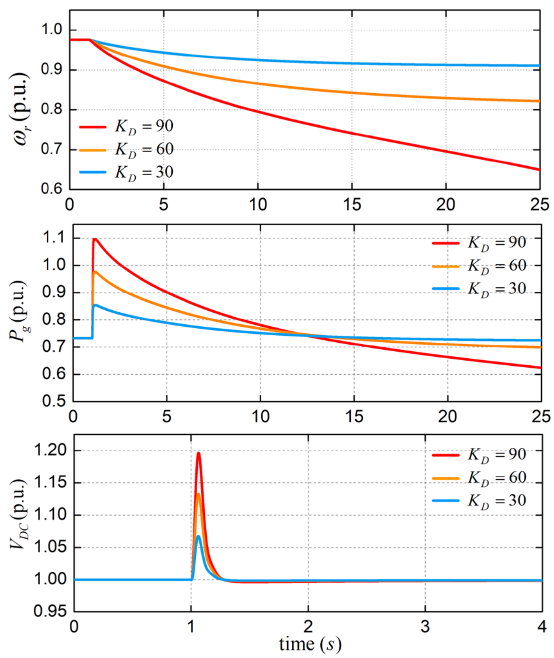

Fig. 10. Time-domain responses of the WT with different values of K_D

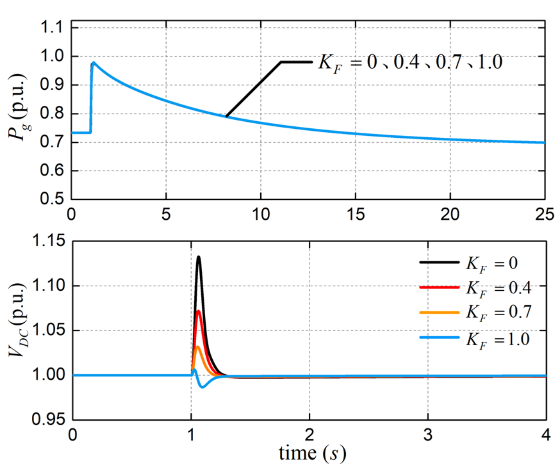

Fig. 11. Time-domain responses of the WT with different values of K_F

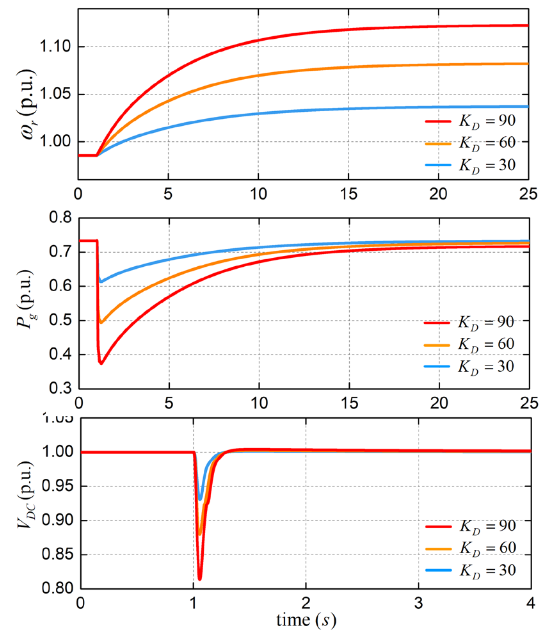

Fig. 12. Time-domain responses of the WT with different values of K_D

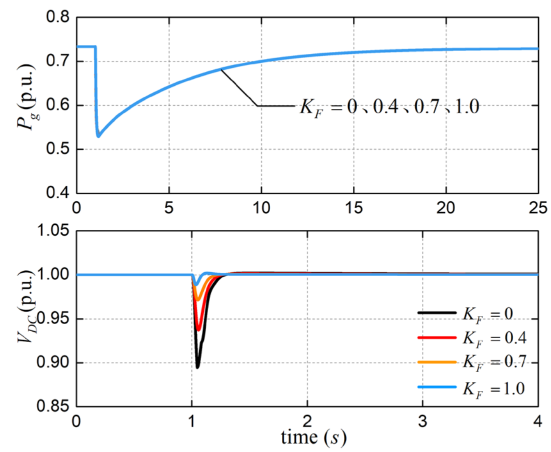

Fig. 13. Time-domain responses of the WT with different values of K_F

VI. Conclusions

In this paper, a current feedforward control (GCFC) scheme was proposed for PMSG-based WTs to suppress the DC-link voltage fluctuations under frequency disturbances. Particularly, we analyzed this DC-link voltage fluctuation phenomenon, which is caused by the power imbalance of the DC-link capacitor due to the effects of the applied frequency droop control. The implementation and mechanism of GCFC were discussed in detail. With the GCFC, the DC-link voltage fluctuation can be kept within its admissible range while the desired frequency support capability of the PMSG-based WT can be ensured. Simulation results were presented to test the dynamic performance of the GCFC when the WT is subjected to grid frequency disturbances.

References

[1] J. Rocabert, A. Luna, F. Blaabjerg, and P. Rodríguez, "Control of Power Converters in AC Microgrids," *IEEE Trans. Power Electron*, vol.27, pp.4734-4749, May 2012.

[2] M. F. M. Arani and Y. A. R. I. Mohamed, "Analysis and Impacts of Implementing Droop Control in DFIG-Based Wind Turbines on Microgrid/Weak-Grid Stability," *IEEE Trans. Power Syst.*, vol. 30, no. 1, pp. 385-396, Jan. 2015

[3] E. Koutroulis and K. Kalaitzakis, "Design of a maximum power tracking system for wind-energy-conversion applications," *IEEE Transaction on Industrial Electronics*, vol. 53, no. 2, pp. 486-494, April 2006.

[4] J. Morren S. W. H. de Haan W. L. Kling J. A. Ferreira "Wind turbines emulating inertia and supporting primary frequency control" *IEEE Trans. Power Syst.,* vol. 21 no. 1 pp. 433-434 Feb. 2006.

[5] L. Huang, H. Xin, L. Zhang, Z. Wang, K. Wu and H. Wang, "Synchronization and Frequency Regulation of DFIG-Based Wind Turbine Generators with Synchronized Control," *IEEE Transaction on Energy Conversion*, vol. 32, no. 3, pp. 1251-1262, Sept. 2017.

[6] Y. C. Xue and N. L. Tai, "Review of contribution to frequency control through variable speed wind turbine," *Renewable Energy*, vol. 36, pp. 1671-1677, Jun 2011.

[7] R. G. de Almeida and J. A. P. Lopes, "Participation of doubly fed induction wind generators in system frequency regulation," *IEEE Transactions on Power Systems*, vol. 22, pp. 944-950, Aug 2007

[8] W. Yi, M. Jianhui, Z. Xiangyu, and X. Lie, "Control of PMSG-Based Wind Turbines for System Inertial Response and Power Oscillation Damping," *IEEE Transaction on Sustainable Energy*, vol. 6, pp. 565-574, 2015

[9] J. V. d. Vyver, J. D. M. D. Kooning, B. Meersman, L. Vandevelde, and T. L. Vandoorn, "Droop Control as an Alternative Inertial Response Strategy for the Synthetic Inertia on Wind Turbines," *IEEE Trans. Power Syst.*, vol. 31, pp. 1129-1138, 2016.

[10] A. Uehara, A. Pratap, T. Goya, T. Senjyu, A. Yona, et al., "A Coordinated Control Method to Smooth Wind Power Fluctuations of a PMSG-Based WECS," *IEEE Transaction on Energy Convers.*, vol. 26, pp. 550-558, Jun 2011

[11] J. Yao, M. Yu, W. Gao and X. Zeng, "Frequency regulation control strategy for PMSG wind-power generation system with flywheel energy storage unit," *IET Renewable Power Generation*, vol. 11, no. 8, pp. 1082-1093, 6 28 2017.

[12] Y. Li, Z. Xu and K. P. Wong, “Advanced Control Strategies of PMSG-Based Wind Turbines for System Inertia Support,” *IEEE Transaction on Power Systems*, DOI: 10.1109/TPWRS.2016.2616171, early access, 2016.

[13] A.D. Hansen, F. Iov, P. Sørensen, N. Cutululis, C. Jauch, and F. Blaabjerg, "Dynamic wind turbine models in power system simulation tool", DIgSILENT Project Report Risø-R-1400(ed.2) (EN).

[14] S. D'Arco, J. A. Suul, O. B. Fosso, "A Virtual Synchronous Machine Implementation for Distributed Control of Power Converters in SmartGrids," *Electric Power System Research*, Vol. 122, May 2015, pp. 180-197.

[15] J. Wang, N. Chang, X. Feng, and A. Monti, “Design of a Generalized Control Algorithm for Parallel Inverters for Smooth Microgrid Transition Operation,” *IEEE Trans. Ind. Electron.*, vol. 62, no. 8, pp. 4900-4914, Aug. 2015

[16] J. Rocabert, A. Luna, F. Blaabjerg, and P. Rodr´ıguez, “Control of power converters in AC microgrids,” *IEEE Trans. Power Electron.*, vol. 27, no. 11, pp. 4734–4749, Nov. 2012.

[17] M. Chinchilla, S. Arnaltes and J. C. Burgos, "Control of permanent-magnet generators applied to variable-speed wind-energy systems connected to the grid," *IEEE Trans. Energy Convers.*, vol. 21, no. 1, pp. 130-135, March 2006.

[18] H. Huang, C. Mao, J. Lu and D. Wang, "Small-signal modelling and analysis of wind turbine with direct drive permanent magnet synchronous generator connected to power grid," *IET Renewable Power Generation*, vol. 6, no. 1, pp. 48-58, January 2012.

[19] J. Hu, Q. Hu, B. Wang, H. Tang and Y. Chi, "Small Signal Instability of PLL-Synchronized Type-4 Wind Turbines Connected to High-Impedance AC Grid During LVRT," *IEEE Trans. Energy Conversion*, vol. 31, no. 4, pp. 1676-1687, Dec. 2016.

[20] Sigurd Skogestad and Ian Postletwaite, “MutiVariable Feedback Control Analysis and Design,” *JOHN WILEY and SONS*(ed.2) (EN)

Jiafa He was born in Sichuan, China, in 1993. He received the bachelor’s degree from the College of Electrical Engineering, Zhejiang University, Hangzhou, China, in 2016, where he is currently working toward the master degree. His research interests include distributed generation and control, renewable energy generation.

Linbin Huang received the B. Eng. degree in College of Electrical Engineering, Zhejiang University, Hangzhou, China, in 2015, where he is currently working toward the Ph.D. degree. His research interests include stability analysis and control of grid-connected power converters.

Huanhai Xin received the Ph.D. degree College of Electrical Engineering, Zhejiang University, Hangzhou, China, in June 2007. He was a post-doctor in the Electrical Engineering and Computer Science Department of the University of Central Florida, Orlando, from June 2009 to July 2010. He is currently a Professor in the Department of Electrical Engineering, Zhejiang University. His research interests include distributed control in active distribution grid and micro-gird, AC/DC power system transient stability analysis and control, and grid-integration of large-scale renewable energy to weak grid.